JCTC Journal of Chemical Theory and Computation

Article

pubs.acs.org/JCTC

Electronic Band Shapes Calculated with Optimally Tuned Range-Separated Hybrid Functionals

Barry Moore, II,[†,∥] Azzam Charaf-Eddin,[‡,∥] Aurélien Planchat,[‡] Carlo Adamo,[⊥,§] Jochen Autschbach,*[,†] and Denis Jacquemin*[,‡,§]

[†]Department of Chemistry, University at Buffalo, State University of New York, 359 Natural Sciences Complex, Buffalo, New York 14260-3000, United States

[‡]Laboratoire CEISAM - UMR CNRS 6230, Université de Nantes, 2 Rue de la Houssinière, BP 92208, 44322 Nantes Cedex 3, France

[⊥]Laboratoire LECIME - UMR CNRS 7575, Chimie-ParisTech, 11 rue P. et M. Curie, F-75231 Paris Cedex 05 France

[§]Institut Universitaire de France, 103, bd Saint-Michel, F-75005 Paris Cedex 05, France

Supporting Information

ABSTRACT: Using a set of 20 organic molecules, we assess the accuracy of both the absorption and emission band shapes obtained by two optimally tuned range-separated hybrid functionals possessing 0% (LC-PBE*) and 25% (LC-PBE0*) of short-range exact exchange as well as by four other hybrid functionals including or not dispersion and long-range corrections (APF-D, PBE0-1/3, SOGGA11-X, and ωB97X-D). The band topologies are compared to experimental data and to previous time-dependent density functional theory calculations. It turns out that both optimally tuned functionals vastly improve the vibronic band shapes obtained with the non-tuned LC-PBE approach but, statistically, do not yield more accurate topologies than standard hybrid functionals. In other words, optimal tuning allows to obtain more accurate excited-state energies without degrading the description of band shapes. In addition, the LC-PBE0* 0−0 energies have been determined for a set of 40 compounds, and it is shown that the results are, on average, less accurate than those obtained by LC-PBE* for the same panel of molecules. The correlation between the optimal range-separation parameters determined for LC-PBE* and LC-PBE0* is discussed as well.

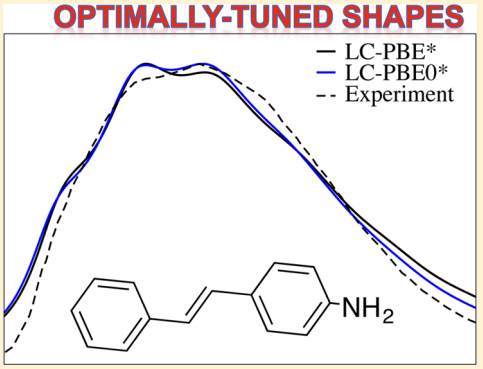

1. INTRODUCTION

Time-dependent density functional theory (TD-DFT)[1] encompasses the generalization of density functional theory (DFT) to time-dependent external potentials, allowing the characterization of electronically excited-state (ES) and frequency-dependent molecular properties via explicitly time-dependent calculations or by using frequency-dependent response theory.[2−4] TD-DFT has become the standard approach to model the optical spectra of both organic and inorganic dyes.[5] This success parallels the popularity of DFT for ground-state (GS) properties and has been made possible by efficient implementations of the TD-DFT linear-response formalism for excitation spectra[2,6−9] that paved the way to computations on large systems.

However, direct comparisons of the theoretical ES data with experimental measurements remain challenging. For instance, for simulating simple experimental absorption and fluorescence spectra one needs to obtain 0−0 energies (corresponding to the AFCP, that is, the absorption fluorescence crossing point) and/or band topologies. Unlike the vertical electronic transition energies produced by typical ES calculations, such simulations can be compared directly with experimental results. Both 0−0 energies and band shape simulations imply the computation of the GS and ES vibrational spectrum and, consequently, require access to the ES Hessian. Even though analytic implementations of the TD-DFT ES Hessian became available recently,[10,11] its computation remains a significant computational bottleneck for large systems. Moreover, the accuracy of TD-DFT computations of ES data is critically dependent on the exchange−correlation functional (XCF).[12]

There are a number of works devoted to the quest of finding the best default XCF for calculating 0−0 energies of small and medium-sized molecules;[13−23] the main common findings of these studies have been summarized in a recent review.[12] On the contrary, much fewer broad-scope benchmarks have been performed for band shapes that require the additional determination of vibronic couplings, typically through Franck−Condon and/or Herzberg−Teller approaches. Indeed, while several works devoted to (very) specific vibronic scenarii (molecules or functionals) have appeared,[24−43] general benchmarks remain scarce. To the best of our knowledge, the two broadest investigations are a 2004 study of Dierksen and Grimme[14] and our 2013 work.[44] In the former, the authors

Received: August 5, 2014

   dx.doi.org/10.1021/ct500712w | J. Chem. Theory Comput. XXXX, XXX, XXX−XXX

Scheme 1. Set of Molecules Used for the Vibronic Benchmarks[a]

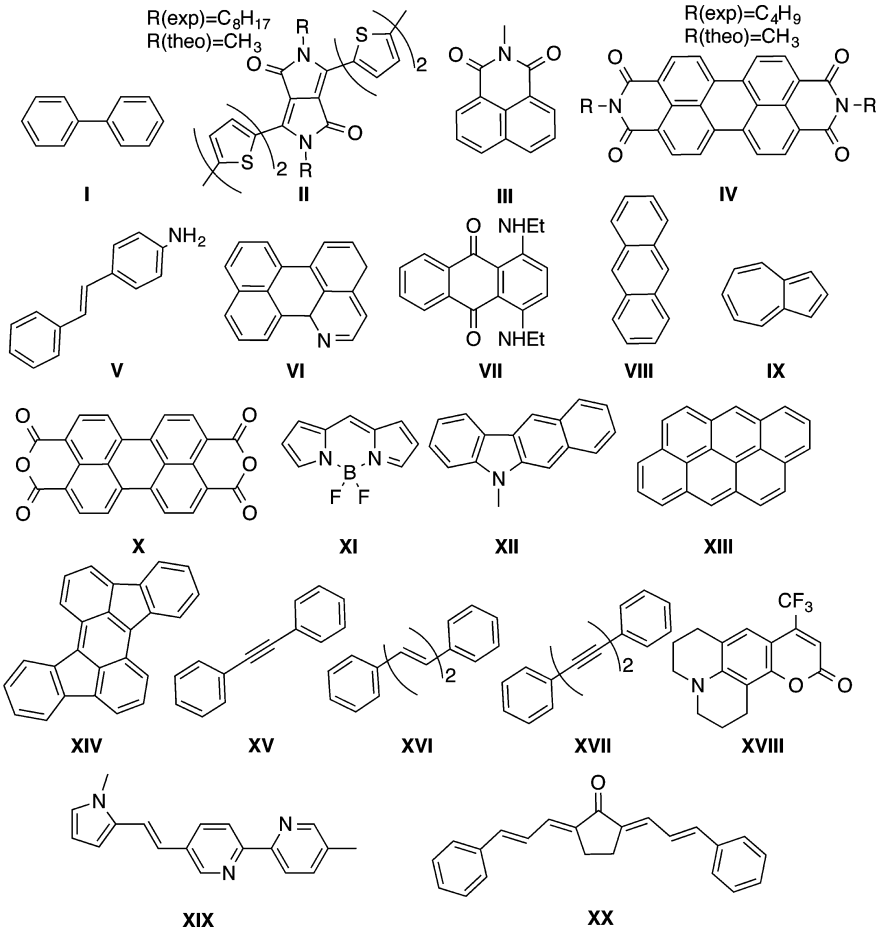

[a]Solvents and experimental references are provided in Table S-I in the SI.

determined gas-phase absorption spectra of 43 organic molecules using three XCF (BP86, B3LYP and BH&HLYP) and concluded that an exact exchange ratio of ca. 30−40% was optimal in (global) hybrid functionals. In the latter, we evaluated the pros and cons of six XCF (B3LYP, PBE0, M06, M06-2X, CAM-B3LYP, and LC-PBE) using the absorption and emission spectra of 20 solvated molecules (see Scheme 1). In that work, we found that most XCF, except LC-PBE, provided relatively similar results, the smallest average deviation of the relative positions of the vibronic maxima being attained with B3LYP. It is noteworthy that the panel of dyes displayed in Scheme 1 contains not only canonical aromatic hydrocarbons but also several "real-life" dyes built around key chromogenic cores, e.g., anthraquinone, coumarin, BODIPY, diketopyrrolopyrole, etc., that all display significantly structured optical spectra. We note that, with the exception of **XVIII**, the lowest excited states investigated here mainly present a valence (localized) nature and do not afford a strong charge-transfer character.[44]

In the present work, we used the lowest dipole-allowed ES for the set of molecules shown in Scheme 1 in order to assess the usefulness of two non-empirically ('optimally') tuned (OT) range-separate exchange (RSE) hybrid functionals in the framework of calculations of band shapes, a task never conducted to date. For comparison, we have also evaluated the performances of four other hybrid XCF devised recently, namely APF-D,[45] PBE0−1/3,[46] SOGGA11-X,[47] and ωB97X-D.[48] The OT approach in its original form[49−51] is based on the fact that in exact Kohn−Sham (KS) and generalized KS theory, the energy of the highest occupied molecular orbital (HOMO), $\varepsilon_H(N)$, for an N-electron system should be equal, except for the sign, to the vertical ionization potential, IP(N). The IP(N) is simply calculated as the energy difference $E(N-1) - E(N)$ for a given XCF and can significantly differ from $-\varepsilon_H(N)$ for approximate XCF.[52] In OT RSE, the range-separation parameter γ is non-empirically adjusted so to be as close as possible to $\varepsilon_H(N) = -\mathrm{IP}(N)$. The IP tuning may be carried out to find an optimal γ for the N and $N + i$ electron species with varying i simultaneously in order to give simple physical interpretations to the energies of the frontier orbitals. The tuning concept was subsequently extended[53,54] to minimize the DFT delocalization error (DE)[55] by non-empirically optimizing a second parameter in the range separation ("two-dimensional tuning") after it was noted that IP-tuned RSE functionals tend to produce a smaller DE than standard XCF. In turn, the DE is the root cause of many of the problems plaguing DFT and TD-DFT calculations. It has been reported that IP-tuned RSE provide both small DE and improved optical gaps.[51,54,56−62]

There is now a rapidly increasing number of studies (see ref 63 for an overview and a worked-out example) showing that non-empirical tuning may lead to vastly improved electronic spectra as well as other response properties obtained from TD-DFT, in particular for cases such as conjugated π-chromophores where the DE can have a large impact on ES

dx.doi.org/10.1021/ct500712w | J. Chem. Theory Comput. XXXX, XXX, XXX−XXX

energies and response properties. In a previous study [22] we have shown that the optimally tuned RSE functional LC-PBE* (see below) afforded the smallest mean unsigned error (MUE) reported so far for 0−0 energies as well as a very good theory/experiment correlation. Moreover, great improvement over a standard parametrization of LC-PBE was obtained owing to the fact that range-separation parameters determined for small-molecule benchmark sets are not suitable for extended π-chromophores.[64] However, to date no investigation has been performed for vibrational band shapes. It is important to verify that the use of OT functionals improves, as expected, the energetic description but does not deteriorate the quality of other simulated spectral parameters—chiefly among them the shapes of the absorption and emission bands.

2. METHODOLOGY

2.1. Finding Optimal Range-Separation Parameters. The RSE tuning has been carried out using the error-function range-separation approach[65−67]

$$\frac{1}{r_{12}} = \frac{\alpha + \beta\ \mathrm{erf}(\gamma r_{12})}{r_{12}} + \frac{1 - [\alpha + \beta\ \mathrm{erf}(\gamma r_{12})]}{r_{12}} \quad (1)$$

in conjunction with the Perdew−Burke−Ernzerhof (PBE)[67] XCF. Here, α and $\alpha + \beta$ correspond to the fraction of exact exchange in the RSE kernel at short and long interelectronic distances r_{12}, respectively. As explained elsewhere,[68] IP tuning for isolated molecules apparently requires the use of a fully long-range corrected (LC) functional with $\alpha + \beta = 1$. For each molecule, two IP-tuned forms of a long-range corrected PBE-based functional, LC-PBE, denoted LC-PBE* ($\alpha = 0.00$, $\beta = 1.00$) and LC-PBE0* ($\alpha = 0.25$,$\beta = 0.75$), the second containing one-quarter of short-range exact exchange, have been obtained by minimizing J^2 of eq 2,

$$J^2 = \sum_{i=0}^{1} [\varepsilon_H(N+i) + \mathrm{IP}(N+i)]^2 \quad (2)$$

with respect to the range-separation parameter γ. As explained in the Introduction, the IP for a given γ is calculated from the difference of total energies, i.e., $\mathrm{IP}(N) = E(N-1) - E(N)$. The two OT functionals are representative cases with different fractions of short-range exact exchange. A two-dimensional tuning would consider all possible α values (under the LC constraint), but since the computational effort for the band-shape simulations is already very high we leave further exploration of different α parameters for a subsequent study. For additional technical details regarding the tuning procedure and further references, see refs 53 and 61−63.

2.2. Computing the AFCP. The method used to obtain the AFCP energies is the same as in our previous study[22] and was extensively tested elsewhere.[20] We therefore only describe the main equations, using eq and neq for the equilibrium and non-equilibrium limits of the selected environmental model, respectively. cLR[69] and LR,[70,71] respectively, indicate the corrected linear-response and the linear-response approximations for the solvent approach (see Section 3). The best estimates of the AFCP energies were determined as

$$E^{\mathrm{AFCP}} = E^{\mathrm{adia}}_{\mathrm{SBS}}(\mathrm{cLR, eq}) + [E^{\mathrm{adia}}_{\mathrm{LBS}}(\mathrm{LR, eq}) - E^{\mathrm{adia}}_{\mathrm{SBS}}(\mathrm{LR, eq})] + \Delta E^{\mathrm{ZPVE}}_{\mathrm{SBS}}(\mathrm{LR, eq}) + \Delta E^{\mathrm{neq/eq}}_{\mathrm{SBS}}(\mathrm{cLR}) \quad (3)$$

where SBS and LBS are the small and large atomic basis sets applied (see Section 2.3). The adiabatic energies are the energy difference between the two states at their respective optimal geometries (R):

$$E^{\mathrm{adia}}_{\mathrm{BS}}(\mathrm{X, eq}) = E^{\mathrm{ES}}_{\mathrm{BS}}(R^{\mathrm{ES}}, \mathrm{X, eq}) - E^{\mathrm{GS}}_{\mathrm{BS}}(R^{\mathrm{GS}}, \mathrm{eq}) \quad (4)$$

and the ZPVE difference between the two states is

$$\Delta E^{\mathrm{ZPVE}}_{\mathrm{BS}}(\mathrm{LR, eq}) = E^{\mathrm{ZPVE}}_{\mathrm{BS}}(R^{\mathrm{ES}}, \mathrm{LR, eq}) - E^{\mathrm{ZPVE}}_{\mathrm{BS}}(R^{\mathrm{GS}}, \mathrm{eq}) \quad (5)$$

The last term is needed to go from equilibrium 0−0 energies to non-equilibrium AFCP energies, and it reads:

$$\Delta E^{\mathrm{neq/eq}}_{\mathrm{BS}}(\mathrm{cLR}) = \frac{1}{2}[\Delta E^{\mathrm{abso-neq/eq}}_{\mathrm{BS}}(\mathrm{cLR}) + \Delta E^{\mathrm{fluo-neq/es}}_{\mathrm{BS}}(\mathrm{cLR})] \quad (6)$$

$$\Delta E^{\mathrm{abso-neq/eq}}_{\mathrm{BS}}(\mathrm{cLR}) = E^{\mathrm{ES}}_{\mathrm{BS}}(R^{\mathrm{GS}}, \mathrm{cLR, neq}) - E^{\mathrm{ES}}_{\mathrm{BS}}(R^{\mathrm{GS}}, \mathrm{cLR, eq}) \quad (7)$$

$$\Delta E^{\mathrm{fluo-neq/eq}}_{\mathrm{BS}}(\mathrm{cLR}) = E^{\mathrm{GS}}_{\mathrm{BS}}(R^{\mathrm{ES}}, \mathrm{eq}) - E^{\mathrm{GS}}_{\mathrm{BS}}(R^{\mathrm{ES}}, \mathrm{cLR, neq}) \quad (8)$$

In this work, the AFCP energies are used both as an input for the vibronic calculations and as a benchmarked property (see Section 4.2).

2.3. Vibronic Couplings. The vibronic couplings have been determined within the Franck−Condon (FC) approximation,[72,73] applied considering the harmonic approximation for the vibrations of both the initial and final states. Note that we only considered strongly dipole-allowed ES here, so that the Herzberg−Teller corrections can be neglected. In fact, different harmonic FC models are possible, namely the vertical and adiabatic schemes (see VH and AH in ref 74). These two schemes provide the same description of the potential energy surface (PES) of the initial state but differ for its final counterpart. In VH, the PES of the final state is built only from the initial state data, i.e., the expansion of the PES of final state is performed around the equilibrium geometry of the initial state. In contrast, in the AH approximation that we used here, one expands the PES of the final state around its equilibrium geometry. A complete comparison between these two models has been performed recently.[74] Note that in the following, the experimental fluorescence spectra measured in the wavelength scale have been transformed in line shapes by applying an intensity correction proportional to ω^2,[75] as this correction, that allows consistent theory/experiment comparisons, significantly affects the band shapes.[76]

3. COMPUTATIONAL DETAILS

Except for the RSE tuning and vibronic calculations, all computations have been performed with the latest version of the Gaussian package.[77] We have systematically applied the highest possible point group symmetry, under the dual conditions that both states present the same point group and that the obtained structures correspond to true minima of the PES. We have improved upon the default thresholds for both the geometry optimization (tight, corresponding to a residual rms force smaller than 10^{-5} au) and energy convergence (at least 10^{-9} au) as well as upgraded the default DFT integration grids: a grid with 99 radial shells and 590 angular points per shell (ultrafine grid in Gaussian09) was systematically used but for the coupled-perturbed KS part that relied on a slightly smaller grid (fine grid corresponding to 75 radial shells and 302

dx.doi.org/10.1021/ct500712w | J. Chem. Theory Comput. XXXX, XXX, XXX−XXX

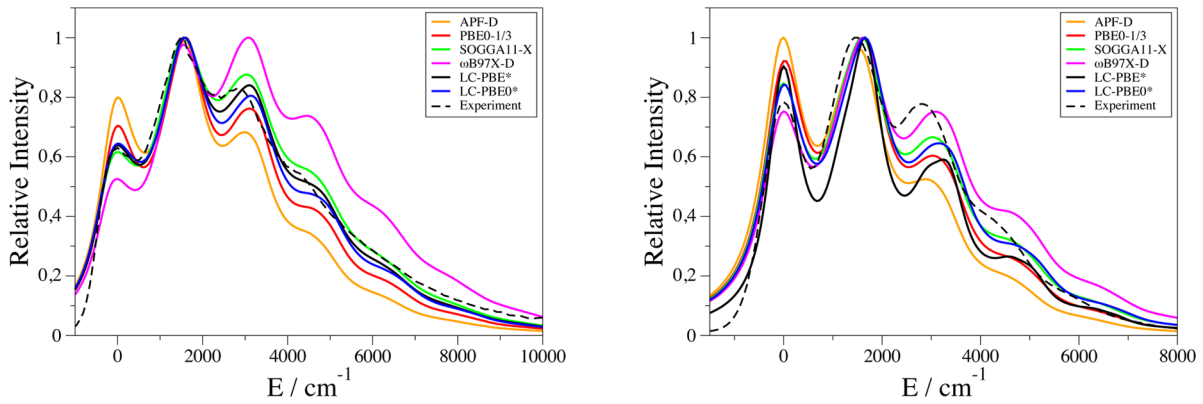

Figure 1. Absorption (left) and emission (right) spectra of **XVI** computed with several XCF. Experimental data taken in ref 84. Note that with LC-PBE0*, the absorption FC convergence of the absorption spectra does not attain 0.9 (see Table S-IV in the SI). As stated in the text, the 0−0 energies has been set to 0 cm^{-1}.

angular points per shell). The GS and ES geometries have been optimized with DFT and TD-DFT, starting from the optimal CAM-B3LYP structures available in the Supporting Information of ref 20, and the vibrational frequencies of both states have been subsequently determined. All structures, presented below, correspond to true minima.[78] Following ref 20, 6-31+G(d) and 6-311++G(2df,2p) have been used as SBS and LBS, respectively, whereas metallic atoms have been described with LANL2DZ.[79,80] The polarizable continuum model (PCM)[81] was used to model bulk solvation effects, using the LR approach[70,71] for both geometry optimizations and frequency calculations and the cLR scheme[69] for total and transition energies. In addition to the optimally tuned XCF, LC-PBE* and LC-PBE0*, we have tested several additional functionals compared to our previous works:[20,22,44] APF-D[45] and PBE0−1/3[46] for both 0−0 energies and band shapes as well as SOGGA11-X[47] and ωB97X-D[48] for band shapes. These additional functionals have been selected to cover, together with our original set (B3LYP, PBE0, M06, M06-2X, CAM-B3LYP and LC-PBE), a large range of XCF nature. Indeed, APF-D is a low exact exchange (22.95%) but includes a corrective term for dispersion effects;[45] PBE0−1/3 is a variant of the well-known PBE0 XCF containing 33.33% of exact exchange[46] in the range of the optimal ratio reported by Grimme (see Introduction); SOGGA11-X is a broad scope XCF containing 40.15% of exact exchange;[47] ωB97X-D is a RSE XCF with a small γ value (0.2 au to be compared to 0.33 au in CAM-B3LYP for instance), a correct asymptotic behavior and an empirical correction for dispersion effects.[48]

The optimal range-separation parameters have been determined using a developers' version of NWChem[82] and applying the 6-31+G(d) atomic basis set for all atoms, except for zinc and osmium where the LANL2DZ basis set and matching effective core potential were used.[79,80] A series of single-point energy calculations with the LC-PBE RSE XCF, in two parametrizations $\alpha = 0.0, \beta = 1.0$ and $\alpha = 0.25, \beta = 0.75$, were carried out for the anion, cation, and neutral systems with varying γ values to minimize J^2 of eq 2. These calculations employed the "xfine" numerical integration grid and an energy convergence of 10^{-8} Hartree. It was demonstrated in our previous work that the optimal range-separation parameters are not strongly dependent on the optimization level used for geometries.[22] Complementing these findings, a recent publication showed that GS geometries and vibrational frequencies of molecules from the G2 benchmark set did not deteriorate when an OT functional was used, although the B3LYP global hybrid performed somewhat better.[83] This finding is in line with long established protocol for response property calculations where exact-exchange rich global hybrids are often found to perform well in the response step, while hybrids with more common fractions of exact exchange or even non-hybrid functionals give better minimum GS geometries.

Starting from the harmonic vibrational spectra of the GS and ES determined with Gaussian09, the vibrationally resolved spectra were computed using the FCclasses program.[25,27,28] The reported spectra have been simulated using convoluting Gaussian functions presenting a half width at half-maximum (HWHM) that has been adjusted to allow meaningful comparisons with experiments (typical value: 0.04 eV). A maximal number of 25 overtones for each mode and 20 combination bands on each pair of modes were included in the calculations. The maximum number of integrals to be computed for each class was set between a minimal value of 10^6 and a maximal value of 10^{12} to obtain the largest possible FC factors (see discussion below). For the vibronic benchmarks, we have systematically set the first (absorption or fluorescence) band to zero and evaluated both the relative intensities of all maxima and the energies of the following peaks in order to quantify the accuracy of each XCF without interferences from the accuracy of the 0−0 energies. In our figures below, and in the SI, fluorescence spectra were mirror-transformed to allow easy comparisons with the corresponding absorption spectra.

4. RESULTS

4.1. Band Shapes. *4.1.1. Convergence of the FC Calculations.* Prior to analyzing the results, it is mandatory to ascertain the convergence of FC calculations. First, we found that biphenyl (molecule **I**) hardly provides converged results because the ES (planar) and the GS (strongly twisted) structures are extremely different. Therefore, this molecule was excluded from the statistical analysis. Second, we have checked that the determinant of the transformation matrix is close to 1. The values can be found in the SI (Table S-II) for both APF-D and LC-PBE*; the smallest determinant obtained is 0.994. Likewise, the overlap between the ground vibrational states of the initial and final electronic states, that should exceed 10^{-4}, is always much larger (smallest value 0.153, see SI, Table S-III). The most difficult parameter to reach is clearly the FC factor that indicates how much of the total vibronic spectrum is

dx.doi.org/10.1021/ct500712w | J. Chem. Theory Comput. XXXX, XXX, XXX−XXX

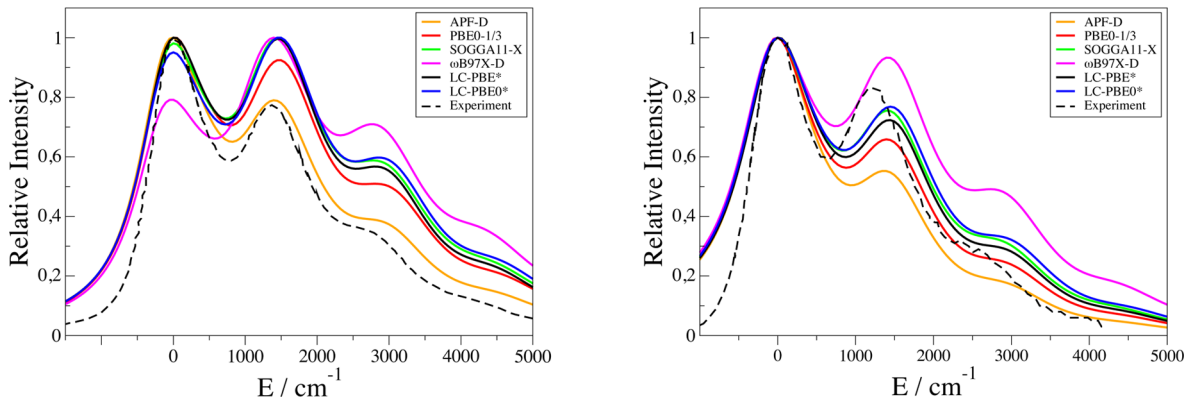

Figure 2. Absorption (left) and emission (right) spectra of **IV** computed with several XCF. Experimental data taken in ref 85. As stated in the text, the 0−0 energies has been set to 0 cm^{-1}.

Table 1. Statistical Analysis Obtained from a Comparison of the Theoretical and the Experimental Absorption Spectra[a]

	positions						intensities					
XCF	MSE	MUE	RMS	SD	max(+)	max(−)	MSE	MUE	RMS	SD	max(+)	max(−)
B3LYP	51	80	102	89	238	−180	−0.07	0.12	0.16	0.15	0.34	−0.38
APF-D	57	112	150	140	453	−326	−0.03	0.09	0.13	0.13	0.33	−0.29
PBE0−1/3	89	134	170	147	453	−326	−0.02	0.09	0.12	0.12	0.38	−0.39
SOGGA11-X	75	117	151	132	453	−326	0.00	0.08	0.12	0.12	0.31	−0.25
CAM-B3LYP	88	108	144	115	472	−121	−0.01	0.13	0.17	0.17	0.62	−0.33
ωB97X-D	57	107	141	130	453	−270	0.01	0.11	0.15	0.15	0.39	−0.25
LC-PBE*	93	121	159	130	453	−171	−0.01	0.10	0.13	0.13	0.29	−0.30
LC-PBE0*	120	139	176	132	453	−171	0.00	0.11	0.14	0.14	0.32	−0.27
LC-PBE	172	182	219	137	553	−180	0.01	0.22	0.27	0.27	0.55	−0.45

[a]Left: relative positions of the bands (in cm^{-1}). Right: relative intensities of the main peaks (arb. units, most intense band set to 1). B3LYP, CAM-B3LYP and LC-PBE values are taken from ref 44.[86].

Table 2. Statistical Analysis Obtained from a Comparison of the Theoretical and the Experimental Fluorescence Spectra[a]

	positions						intensities					
XCF	MSE	MUE	RMS	SD	Max(+)	Max(−)	MSE	MUE	RMS	SD	Max(+)	Max(−)
B3LYP	80	225	291	286	531	−722	−0.09	0.16	0.22	0.20	0.55	−0.45
APF-D	12	194	259	265	343	−725	−0.07	0.12	0.16	0.15	0.24	−0.33
PBE0−1/3	47	227	283	286	393	−725	−0.03	0.09	0.12	0.12	0.24	−0.24
SOGGA11-X	60	229	276	276	394	−673	0.00	0.07	0.11	0.11	0.24	−0.26
CAM-B3LYP	129	242	287	262	446	−623	0.01	0.07	0.12	0.12	0.38	−0.32
ωB97X-D	60	211	287	308	394	−673	0.02	0.07	0.11	0.12	0.26	−0.24
LC-PBE*	104	240	307	305	448	−725	−0.02	0.09	0.12	0.13	0.24	−0.30
LC-PBE0*	87	235	294	287	446	−725	0.00	0.08	0.12	0.12	0.24	−0.28
LC-PBE	229	351	391	326	644	−571	0.04	0.12	0.17	0.17	0.39	−0.29

[a]See footnote of Table 1 for more details.

recovered by the FCclasses program. Table S−IV in the SI provides this factor for the 210 spectra treated when considering all XCF and molecules as well as both absorption and emission. In most cases, the FC factor is converged (>0.9), but in less than 10% of the cases (18 out of 210) this convergence could not be achieved even with 10^{12} integrals. Although we provide figures for these 18 cases in the SI, they have been excluded from our statistical analysis and are not discussed in the following. The interested reader will find further tests of the impact of solvation, temperature, atomic basis set, DFT integration grid in ref 44, and the same holds for the influence of the number of overtones and combination bands used.

4.1.2. Case Studies. Before going to a statistical analysis, let us first discuss a few selected examples of vibronic spectra. Figures of band shapes for all molecules are available in the SI. Vertical values for several XCF and compounds can be found in the SI of ref 22. In Figure 1, we present the absorption and emission spectra obtained for **XVI**,[84] a typical π-conjugated hydrocarbon derivative. For absorption, the relative intensity of the first peak is overestimated by both APF-D and PBE0−1/3 and underestimated by ωB97X-D, whereas SOGGA11-X and the two OT XCF provide accurate data. For the third absorption maxima, all approaches overshoot the position of the band on the energy scale, its intensity being again the most accurate with SOGGA11-X, LC-PBE*, and LC-PBE0*. The outcome is somewhat different for the corresponding emission (right panel in Figure 1), for which, APF-D and PBE0−1/3 remain relatively poor, whereas ωB97X-D becomes the closest to experiment.

dx.doi.org/10.1021/ct500712w | J. Chem. Theory Comput. XXXX, XXX, XXX−XXX

Scheme 2. Representation of the Set of Molecules Used during the 0−0 Benchmarks[a]

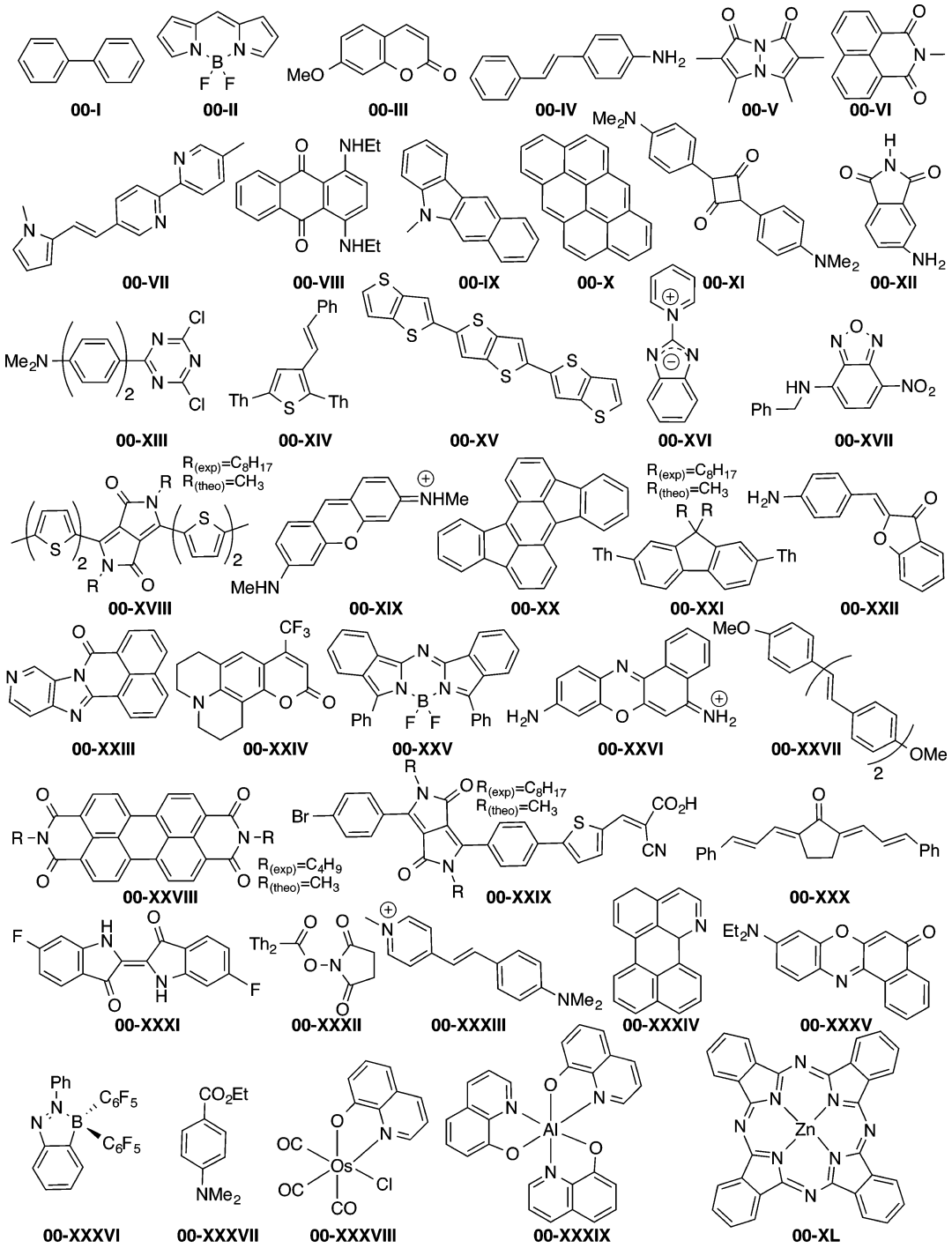

[a]Ph and Th stand for phenyl and thienyl, respectively.

For **IV** (see Figure 2),[85] a perylene diimide typically used in organic electronics, one again obtains that ωB97X-D underestimates the relative intensity of the first absorption band, but in that case, APF-D is clearly the XCF providing the most reliable intensities. All other XCF, optimally tuned or not, overestimate the relative intensities at higher energies. For the emission of **IV**, however, SOGGA11-X and the two OT XCF provide the most accurate spectrum, though again all XCF place the second band at too large energy, an error that we attribute to the use of the harmonic approximation. For these two compounds, we therefore notice that both OT RSE XCF yield results close to each other and similar to the one of SOGGA11-X.

4.1.3. Statistical Analysis. A statistical analysis for all compounds is provided in Tables 1 and 2, for absorption and fluorescence, respectively (a table with joint statistics is available in the SI), together with the results obtained, for the same set, for three previously tested XCF (B3LYP, CAM-

dx.doi.org/10.1021/ct500712w | J. Chem. Theory Comput. XXXX, XXX, XXX−XXX

Table 3. Theoretical AFCP Values in eV[a]

molecule	Opt γ	LC-PBE0*	APF-D	PBE0−1/3	molecule	Opt γ	LC-PBE0*	APF-D	PBE0−1/3
00-I	0.183	4.531	4.309	4.407	**00-XXI**	0.142	3.351	3.068	3.208
00-II	0.178	3.048	2.987	3.052	**00-XXII**	0.163	3.143	2.795	2.991
00-III	0.191	4.036	3.790	3.955	**00-XXIII**	0.161	3.317	2.893	3.133
00-IV	0.166	3.522	3.302	3.431	**00-XXIV**	0.157	3.320	2.939	3.185
00-V	0.178	3.311	3.072	3.258	**00-XXV**	0.115	1.964	1.943	1.982
00-VI	0.185	3.741	3.463	3.610	**00-XXVI**	0.149	2.612	2.503	2.598
00-VII	0.151	3.124	2.855	2.999	**00-XXVII**	0.136	3.061	2.795	2.948
00-VIII	0.151	2.182	2.031	2.156	**00-XXVIII**	0.149	2.424	2.235	2.346
00-IX	0.158	3.331	3.026	3.210	**00-XXIX**	0.125	2.245	1.784	2.077
00-X	0.160	2.870	2.651	2.769	**00-XXX**	0.133	2.725	2.564	2.724
00-XI	0.130	2.440	2.368	2.453	**00-XXXI**	0.153	2.433	2.218	2.386
00-XII	0.200	3.600	3.209	3.445	**00-XXXII**	0.168	3.461	3.271	3.385
00-XIII	0.141	3.125	1.771	2.744	**00-XXXIII**	0.143	2.867	2.535	2.738
00-XIV	0.134	2.997	2.775	2.921	**00-XXXIV**	0.164	2.861	2.624	2.743
00-XV	0.134	2.865	2.631	2.747	**00-XXXV**	0.140	2.666	2.518	2.648
00-XVI	0.182	2.706	2.612	2.055	**00-XXXVI**	0.133	2.892	2.117	2.585
00-XVII	0.170	3.075	2.712	2.964	**00-XXXVII**	0.172	4.290	2.489	4.196
00-XVIII	0.115	2.069	1.907	2.018	**00-XXXVIII**	0.154	2.745	2.468	2.653
00-XIX	0.152	2.994	2.822	2.958	**00-XXXIX**	0.139	2.686	2.445	2.640
00-XX	0.137	2.291	2.098	2.230	**00-XL**	0.113	1.970	1.992	1.991

[a]The optimal γ value (au) used in the LC-PBE0* calculation as well as the solvent are reported for each structure. Molecules are depicted in Scheme 2.

Table 4. Statistical Analysis Obtained from the Comparison of the Theoretical and the Experimental AFCP Energies Listed in Table 3[a]

method	MSE	MUE	RMS	SD	R	max(+)	max(−)
APF-D	0.06	0.27	0.38	0.27	0.79	1.39	−0.64
PBE0	0.03	0.22	0.28	0.17	0.89	0.79	−0.64
PBE0−1/3	−0.14	0.22	0.28	0.18	0.91	0.25	−0.78
M06-2X	−0.25	0.26	0.31	0.18	0.95	0.08	−0.77
LC-PBE*	−0.12	0.20	0.25	0.15	0.93	0.33	−0.68
LC-PBE0*	−0.25	0.26	0.33	0.20	0.93	0.11	−0.81
LC-PBE	−0.56	0.57	0.60	0.20	0.94	0.18	−1.10

[a]All values, but R, are in eV. The PBE0, M06-2X, LC-PBE, and LC-PBE* values have been taken from refs 20 and 22.

B3LYP and LC-PBE).[44] In these tables, we report the mean signed error (MSE, theory-experiment), MUE, root-mean-square deviation (RMS), standard deviation (SD) as well as the maximum discrepancies for both relative positions and heights of the vibronic peaks. As the first band is set to 0.0 cm^{-1} in each case, it has been consequently removed from the statistical analysis. In the SI, Table S-XXVI provides the same information but includes this initial band in the statistics. For the absorption, we first note that MSE is systematically positive, indicating that (harmonic) TD-DFT calculations tend to overshoot the separation between the vibronic peaks. For the positions, the smallest MSE (<60 cm^{-1}) is obtained with B3LYP, APF-D, and ωB97X-D, and all MUE but one (LC-PBE) are within the 90−140 cm^{-1} range. OT vastly improves the default LC-PBE (γ = 0.47) results, as it reduces the MUE by more than 40 cm^{-1}. Among the two OT-RSE XCF, the simpler LC-PBE* provides the most accurate data. However, none of the RSH, optimally tuned or not, is able to outperform B3LYP for band separations. For the relative intensities, several conclusions pertain, i.e., (i) all XCF but LC-PBE give quite similar errors with deviations of ca. 10%; (ii) OT significantly improves the quality of the LC-PBE estimates; and (iii) LC-PBE* and LC-PBE0* do not systematically outperform global hybrids, the smallest deviations being reached with SOGGA11-X.

Consistently, with our previous work,[44] the results of Table 2 indicate that the errors made on the relative emission intensities are in the same line as for absorption but are twice as large for the relative positions of the fluorescence peaks (the deviations are ca. 220 cm^{-1} for emission and ca. 110 cm^{-1} for absorption).[87] APF-D provides the smallest deviations with a MSE (MUE) of 12 (194) cm^{-1} and appears as the most effective XCF for relative positions of the emission bands. As for absorption, both LC-PBE* and LC-PBE0* significantly improve over LC-PBE (MUE smaller by ca. 100 cm^{-1}) and yield average errors comparable to that obtained with ωB97X-D or SOGGA11-X. For the relative intensities, all XCF but B3LYP, APF-D, and LC-PBE provide errors below the 10% threshold.

In the SI (Tables S-XXVII to S-XXXII), one can find a statistical analysis obtained by separating the 8 hydrocarbons and the 12 heteroatomic compounds of Scheme 1 as well as by considering only the two first peaks of each spectrum. In all cases, the main conclusions described above pertain: (i) OT significantly decreases the error obtained with the original LC-PBE but does not lead to improved results compared to other XCF, e.g., ωB97X-D; and (ii) the deviations tend to be larger

dx.doi.org/10.1021/ct500712w | J. Chem. Theory Comput. XXXX, XXX, XXX−XXX

for emission than absorption irrespective of the selected XCF or molecular subset.

4.2. 0−0 Energies. Though numerous benchmarks appeared for 0−0 energies previously,[14−16,18−23] only our 2014 work assessed optimal tuning in that framework using LC-PBE*.[22] For the 40 molecules shown in Scheme 2,[88] it was found that this XCF provides the smallest MUE reported to date.[22] For this reason, we have tested LC-PBE0* in the same framework to determine if the use of non-zero short-range exact exchange improves the estimates. Table 3 lists the optimal γ values and the AFCP energies computed with LC-PBE0*, APF-D, and PBE0−1/3 (the list of solvents and experimental values and references are available in the SI). The results obtained with nine other XCF are available elsewhere.[20,22]

We do not discuss individual cases but instead directly turn toward the statistical analysis using the data listed in Table 4: MSE, MUE, RMS, SD, and extreme deviations as well as the linear correlation coefficient, R, between experimental and theoretical AFCP energies. One clearly notices that APF-D provides a much smaller R, and therefore a larger SD than all other XCF, and this is related to the low-exact exchange percentage included in this global hybrid. Indeed, this family of XCF tends to provide incorrect PESs for the ES which possess a significant charge-transfer nature. This is obvious for **00-XXXVII** for which the terminal amino group in the ES presents a dihedral angle of 90° with respect to the phenyl ring when using APF-D, an unphysical result yielding to a spurious ES of much too small energy (see Table 3). This overtwisting ES problem has been discussed and rationalized before.[89−91] By comparing the results of PBE0 and PBE0−1/3, one notices that increasing the exact exchange ratio in global hybrids (here from 25% to 33%) improves the R without, in that specific case, deteriorating the MUE for similar reasons: some of the cases that present a qualitatively inaccurate ES geometry with PBE0 are corrected with PBE0−1/3. As for the band topologies, it is evident that OT improves the results over the global parametrization of LC-PBE: the MUE is cut in half, while R is almost conserved. LC-PBE* appears to be more accurate than LC-PBE0* for all main statistical parameters. Of the 40 dyes treated, the latter XCF outperforms the former only in 10 cases. In fact, LC-PBE0* provides MSE and MUE equal to the one obtained with M06-2X, the latter being the XCF providing the largest correlation between experiment and theory (R = 0.95).

4.3. Tuning Parameter. In Figure 3, we compare the optimal range-separation parameters γ obtained for LC-PBE* and LC-PBE0* considering both sets of molecules (Schemes 1 and 2). The optimal γ values determined for LC-PBE0* (α = 0.25) are systematically smaller than their counterparts obtained for LC-PBE* (α = 0.00). This trend could be expected: the XCF including short-range exact exchange needs a slower growth of the exact exchange with increasing interelectronic separation. The average variation between the two OT-RSE is −0.052 au with minimal and maximal changes of −0.041 (**00-XXXVIII**) and −0.064 au (**III**), respectively. It is indeed obvious from Figure 3 that the γ values obtained for the two XCF are highly correlated (R = 0.98), so that one could provide an accurate guess from one starting with the other. A justification for using a particular value of α may be derived from minimizing the DE in a two-dimensional tuning procedure. However, as pointed out in Section 2.1, given the size of the molecule set and the size of many of the molecules within the set, there is a large computational overhead involved with this procedure. We plan to address this point in a follow-up study.

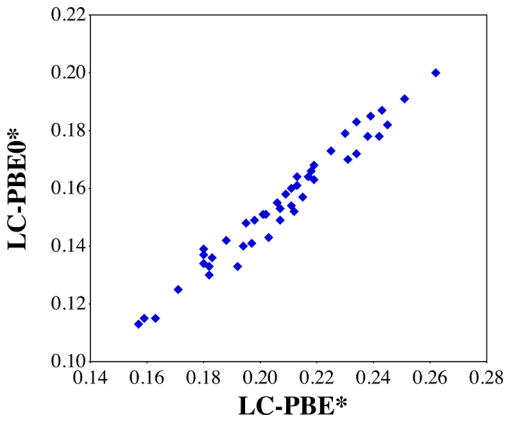

Figure 3. Comparisons between the optimal γ values determined for LC-PBE* and LC-PBE0* for the 46 different molecules investigated here. All values in au.

5. CONCLUSIONS

For the first time, two optimally tuned range-separated hybrids, namely LC-PBE* and LC-PBE0*, have been used for computing vibronic band shapes, and the second XCF was used to obtain 0−0 energies as well. Finding an XCF that is satisfying for these properties is certainly challenging, as one needs a method that simultaneously provides a balanced answer for both the GS and ES structures and force fields as well as the transition energies between these states. In other words, contrary to vertical spectroscopic calculations where one can select a XCF for GS geometries (e.g., B3LYP) and use another XCF depending on the nature of the ESs (e.g., CAM-B3LYP for charge-transfer states), one needs to find, for 0−0 energies and vibronic band shapes, XCF optimal for all properties. To obtain statistically relevant conclusions, we have used large sets of organic molecules and assessed other XCF (APF-D, PBE0−1/3, SOGGA11-X and ωB97X-D). It turns out that optimal tuning vastly improves the results of the default LC-PBE approach, cutting down its errors by a factor of ca. 2 for both energies and band shapes, for the reason that large delocalized π-chromophores require range-separation parameters much smaller than 0.47 (used in the default LC-PBE). In most cases, LC-PBE0* provides less accurate results than LC-PBE*, and when some improvements are found, e.g., for emission band shapes, they are not very significant. We also found that the optimal γ parameters determined for LC-PBE* and LC-PBE0* are highly correlated (R = 0.98). Overall, it seems that LC-PBE* is therefore an interesting compromise approach: it yields the smallest MUE and a large R on 0−0 energies, while providing band shapes with an accuracy comparable to the one obtained with other hybrid XCF. Most importantly, the gains in accuracy achieved via tuning in the energetic description of the chromophores are not accompanied by a deterioration of the quality of the band shapes.

■ ASSOCIATED CONTENT

Supporting Information

List of solvent used for molecules **I**−**XX** together with experimental references. FC convergence test values. Full list of relative positions and intensities for all peaks. Representation of all vibronic spectra and comparisons with experiment.

dx.doi.org/10.1021/ct500712w | J. Chem. Theory Comput. XXXX, XXX, XXX−XXX

Additional statistical analysis. List of solvent used for molecules **00-I−00-XL** together with experimental references. This material is available free of charge via the Internet at http://pubs.acs.org/.

AUTHOR INFORMATION

Corresponding Authors

*E-mail: jochena@buffalo.edu.

*E-mail: Denis.Jacquemin@univ-nantes.fr.

Author Contributions

‖These authors ontributed equally.

Notes

The authors declare no competing financial interest.

ACKNOWLEDGMENTS

A.C.E. and D.J. acknowledge the European Research Council (ERC) and the Région des Pays de la Loire for financial support in the framework of a Starting Grant (Marches -278845) and a recrutement sur poste stratégique, respectively. J.A. and B.M. are grateful for financial support of this research by the National Science Foundation, grant CHE-1265833. This research used resources of (1) the GENCI-CINES/IDRIS, (2) CCIPL (Centre de Calcul Intensif des Pays de Loire), (3) a local Troy cluster, and (4) the Center for Computational Research at SUNY Buffalo. The authors are indebted to the COST program CODECS and its members for support and many helpful discussions, respectively.

REFERENCES

(1) Runge, E.; Gross, E. K. U. *Phys. Rev. Lett.* **1984**, *52*, 997−1000.

(2) Casida, M. E. Time-Dependent Density-Functional Response Theory for Molecules. In *Recent Advances in Density Functional Methods*; Chong, D. P., Ed.; World Scientific: Singapore, 1995; Vol. *1*; pp 155−192.

(3) Elliott, P.; Burke, K.; Furche, F. In *Reviews of Computational Chemistry*; Lipkowitz, K. B., Cundari, T. R., Eds.; Wiley: Hoboken, NJ, 2009.

(4) Autschbach, J. Computational Inorganic and Bioinorganic Chemistry. In *Encyclopedia of Inorganic Chemistry*; Solomon, E. I., Scott, R. A., King, R. B., Eds.; John Wiley & Sons: Chichester, UK, 2009; Vol. *9*; pp 71−90.

(5) Laurent, A. D.; Adamo, C.; Jacquemin, D. *Phys. Chem. Chem. Phys.* **2014**, *16*, 14334−14356.

(6) van Gisbergen, S. J. A.; Snijders, J. G. *J. Chem. Phys.* **1995**, *103*, 9347−9354.

(7) Bauernschmitt, R.; Ahlrichs, R. *Chem. Phys. Lett.* **1996**, *256*, 454−464.

(8) Petersilka, M.; Gossman, U. J.; Gross, E. K. U. *Phys. Rev. Lett.* **1996**, *76*, 1212−1215.

(9) Stratmann, R. E.; Scuseria, G. E.; Frisch, M. J. *J. Chem. Phys.* **1998**, *109*, 8218−8224.

(10) Liu, J.; Liang, W. Z. *J. Chem. Phys.* **2011**, *135*, 014113.

(11) Liu, J.; Liang, W. Z. *J. Chem. Phys.* **2011**, *135*, 184111.

(12) Laurent, A. D.; Jacquemin, D. *Int. J. Quantum Chem.* **2013**, *113*, 2019−2039.

(13) Furche, F.; Ahlrichs, R. *J. Chem. Phys.* **2002**, *117*, 7433−7447.

(14) Dierksen, M.; Grimme, S. *J. Phys. Chem. A* **2004**, *108*, 10225−10237.

(15) Goerigk, L.; Moellmann, J.; Grimme, S. *Phys. Chem. Chem. Phys.* **2009**, *11*, 4611−4620.

(16) Goerigk, L.; Grimme, S. *J. Chem. Phys.* **2010**, *132*, 184103.

(17) Nguyen, K. A.; Day, P. N.; Pachter, R. *Int. J. Quantum Chem.* **2010**, *110*, 2247−2255.

(18) Send, R.; Kühn, M.; Furche, F. *J. Chem. Theory Comput.* **2011**, *7*, 2376−2386.

(19) Bates, J. E. E.; Furche, F. *J. Chem. Phys.* **2012**, *137*, 164105.

(20) Jacquemin, D.; Planchat, A.; Adamo, C.; Mennucci, B. *J. Chem. Theory Comput.* **2012**, *8*, 2359−2372.

(21) Winter, N. O. C.; Graf, N. K.; Leutwyler, S.; Hattig, C. *Phys. Chem. Chem. Phys.* **2013**, *15*, 6623−6630.

(22) Jacquemin, D.; Moore, B.; Planchat, A.; Adamo, C.; Autschbach, J. *J. Chem. Theory Comput.* **2014**, *10*, 1677−1685.

(23) Fang, C.; Oruganti, B.; Durbeej, B. *J. Phys. Chem. A* **2014**, *118*, 4157−4171.

(24) Dierksen, M.; Grimme, S. *J. Chem. Phys.* **2004**, *120*, 3544−3554.

(25) Santoro, F.; Improta, R.; Lami, A.; Bloino, J.; Barone, V. *J. Chem. Phys.* **2007**, *126*, 084509.

(26) Improta, R.; Barone, V.; Santoro, F. *Angew. Chem., Int. Ed. Engl.* **2007**, *46*, 405−408.

(27) Santoro, F.; Improta, R.; Lami, A.; Bloino, J.; Barone, V. *J. Chem. Phys.* **2007**, *126*, 184102.

(28) Santoro, F.; Lami, A.; Improta, R.; Bloino, J.; Barone, V. *J. Chem. Phys.* **2008**, *128*, 224311.

(29) Guthmuller, J.; Zutterman, F.; Champagne, B. *J. Chem. Theory Comput.* **2008**, *4*, 2094−2100.

(30) Andrzejak, M.; Pawlikowski, M. T. *J. Phys. Chem. A* **2008**, *112*, 13737−13744.

(31) Improta, R.; Santoro, F.; Barone, V.; Lami, A. *J. Phys. Chem. A* **2009**, *113*, 15346−15354.

(32) Jacquemin, D.; Peltier, C.; Ciofini, I. *Chem. Phys. Lett.* **2010**, *493*, 67−71.

(33) Jacquemin, D.; Brémond, E.; Planchat, A.; Ciofini, I.; Adamo, C. *J. Chem. Theory Comput.* **2011**, *7*, 1882−1892.

(34) Avila Ferrer, F. J.; Improta, R.; Santoro, F.; Barone, V. *Phys. Chem. Chem. Phys.* **2011**, *13*, 17007−17012.

(35) Chibani, S.; Le Guennic, B.; Charaf-Eddin, A.; Maury, O.; Andraud, C.; Jacquemin, D. *J. Chem. Theory Comput.* **2012**, *8*, 3303−3313.

(36) Jacquemin, D.; Brémond, E.; Ciofini, I.; Adamo, C. *J. Phys. Chem. Lett.* **2012**, *3*, 468−471.

(37) Lopez, G. V.; Chang, C.-H.; Johnson, P. M.; Hall, G. E.; Sears, T. J.; Markiewicz, B.; Milan, M.; Teslja, A. *J. Phys. Chem. A* **2012**, *116*, 6750−6758.

(38) Stendardo, E.; Ferrer, F. A.; Santoro, F.; Improta, R. *J. Chem. Theory Comput.* **2012**, *8*, 4483−4493.

(39) Chibani, S.; Le Guennic, B.; Charaf-Eddin, A.; Laurent, A. D.; Jacquemin, D. *Chem. Sci.* **2013**, *4*, 1950−1963.

(40) Chibani, S.; Charaf-Eddin, A.; Le Guennic, B.; Jacquemin, D. *J. Chem. Theory Comput.* **2013**, *9*, 3127−3135.

(41) Zakrzewska, A.; Zalesny, R.; Kolehmainen, E.; Osmialowski, B.; Jedrzejewska, B.; Agren, H.; Pietrzak, M. *Dyes Pigm.* **2013**, *99*, 957−965.

(42) Balmer, F. A.; Ottiger, P.; Pfaffen, C.; Leutwyler, S. *J. Phys. Chem. A* **2013**, *117*, 10702−10713.

(43) Avila Ferrer, F. J.; Barone, V.; Cappelli, C.; Santoro, F. *J. Chem. Theory Comput.* **2013**, *9*, 3597−3611.

(44) Charaf-Eddin, A.; Planchat, A.; Mennucci, B.; Adamo, C.; Jacquemin, D. *J. Chem. Theory Comput.* **2013**, *9*, 2749−2760.

(45) Austin, A.; Petersson, G. A.; Frisch, M. J.; Dobek, F. J.; Scalmani, G.; Throssell, K. *J. Chem. Theory Comput.* **2012**, *8*, 4989−5007.

(46) Guido, C. A.; Brémond, E.; Adamo, C.; Cortona, P. *J. Chem. Phys.* 2013, *138*, -.

(47) Peverati, R.; Truhlar, D. *J. Chem. Phys.* **2011**, *135*, 191102−191102.

(48) Chai, J. D.; Head-Gordon, M. *Phys. Chem. Chem. Phys.* **2008**, *10*, 6615−6620.

(49) Baer, R.; Livshits, E.; Salzner, U. *Annu. Rev. Phys. Chem.* **2010**, *61*, 85−109.

(50) Stein, T.; Eisenberg, H.; Kronik, L.; Baer, R. *Phys. Rev. Lett.* **2010**, *105*, 266802−4.

(51) Kronik, L.; Stein, T.; Refaely-Ambrason, S.; Baer, R. *J. Chem. Theory Comput.* **2012**, *8*, 1515−1531.

(52) Gritsenko, O. V.; Baerends, E. J. *J. Chem. Phys.* **2004**, *121*, 655−660.

(53) Srebro, M.; Autschbach, J. *J. Phys. Chem. Lett.* **2012**, *3*, 576−581.
(54) Refaely-Abramson, S.; Sharifzadeh, S.; Govind, N.; Autschbach, J.; Neaton, J. B.; Baer, R.; Kronik, L. *Phys. Rev. Lett.* **2012**, *109*, 226405−5.
(55) Cohen, A. J.; Mori-Sánchez, P.; Yang, W. *Science* **2008**, *321*, 792−794.
(56) Refaely-Ambrason, S.; Baer, R.; Kronik, L. *Phys. Rev. B* **2011**, *84*, 075144.
(57) Moore, B., II; Autschbach, J. *ChemistryOpen* **2012**, *1*, 184−194.
(58) Moore, B., II; Srebro, M.; Autschbach, J. *J. Chem. Theory Comput.* **2012**, *8*, 4336−4346.
(59) Gledhill, J. D.; Peach, M. J. G.; Tozer, D. J. *J. Chem. Theory Comput.* **2013**, *9*, 4414−4420.
(60) Moore, B., II; Autschbach, J. *J. Chem. Theory Comput.* **2013**, *9*, 4991−5003.
(61) Sun, H.; Autschbach, J. *ChemPhysChem* **2013**, *14*, 2450−2461.
(62) Sun, H.; Autschbach, J. *J. Chem. Theory Comput.* **2014**, *10*, 1035−1047.
(63) Autschbach, J.; Srebro, M. *Acc. Chem. Res.* **2014**, *47*, 2592−2602.
(64) Körzdörfer, T.; Sears, J. S.; Sutton, C.; Brédas, J.-L. *J. Chem. Phys.* **2011**, *135*, 204107−6.
(65) Savin, A. In *Recent Developments and Applications of Modern Density Functional Theory*; Seminario, J. M., Ed.; Elsevier: Amsterdam, 1996; Chapter 9, pp 327−354.
(66) Iikura, H.; Tsuneda, T.; Yanai, T.; Hirao, K. *J. Chem. Phys.* **2001**, *115*, 3540−3544.
(67) Yanai, T.; Tew, D. P.; Handy, N. C. *Chem. Phys. Lett.* **2004**, *393*, 51−56.
(68) Perdew, J. P.; Burke, K.; Ernzerhof, M. *Phys. Rev. Lett.* **1996**, *77*, 3865−3868.
(69) Caricato, M.; Mennucci, B.; Tomasi, J.; Ingrosso, F.; Cammi, R.; Corni, S.; Scalmani, G. *J. Chem. Phys.* **2006**, *124*, 124520.
(70) Cammi, R.; Mennucci, B. *J. Chem. Phys.* **1999**, *110*, 9877−9886.
(71) Cossi, M.; Barone, V. *J. Chem. Phys.* **2001**, *115*, 4708−4717.
(72) Franck, J. *Trans. Faraday Soc.* **1926**, *21*, 536−542.
(73) Condon, E. *Phys. Rev.* **1928**, *32*, 858−872.
(74) Avila Ferrer, F. J.; Santoro, F. *Phys. Chem. Chem. Phys.* **2012**, *14*, 13549−13563.
(75) Valeur, B. *Molecular Fluorescence: Principles and Applications*; Wiley-VCH: Weinheim, 2002.
(76) Avila Ferrer, F. J.; Cerezo, J.; Stendardo, E.; Improta, R.; Santoro, F. *J. Chem. Theory Comput.* **2013**, *9*, 2072−2082.
(77) Frisch, M. J.; Trucks, G. W.; Schlegel, H. B.; Scuseria, G. E.; Robb, M. A.; Cheeseman, J. R.; Scalmani, G.; Barone, V.; Mennucci, B.; Petersson, G. A.; Nakatsuji, H.; Caricato, M.; Li, X.; Hratchian, H. P.; Izmaylov, A. F.; Bloino, J.; Zheng, G.; Sonnenberg, J. L.; Hada, M.; Ehara, M.; Toyota, K.; Fukuda, R.; Hasegawa, J.; Ishida, M.; Nakajima, T.; Honda, Y.; Kitao, O.; Nakai, H.; Vreven, T.; Montgomery, J. A., Jr.; Peralta, J. E.; Ogliaro, F.; Bearpark, M.; Heyd, J. J.; Brothers, E.; Kudin, K. N.; Staroverov, V. N.; Kobayashi, R.; Normand, J.; Raghavachari, K.; Rendell, A.; Burant, J. C.; Iyengar, S. S.; Tomasi, J.; Cossi, M.; Rega, N.; Millam, J. M.; Klene, M.; Knox, J. E.; Cross, J. B.; Bakken, V.; Adamo, C.; Jaramillo, J.; Gomperts, R.; Stratmann, R. E.; Yazyev, O.; Austin, A. J.; Cammi, R.; Pomelli, C.; Ochterski, J. W.; Martin, R. L.; Morokuma, K.; Zakrzewski, V. G.; Voth, G. A.; Salvador, P.; Dannenberg, J. J.; Dapprich, S.; Daniels, A. D.; Farkas, O.; Foresman, J. B.; Ortiz, J. V.; Cioslowski, J.; Fox, D. J. *Gaussian 09*, revision D.01.; Gaussian Inc.: Wallingford CT, 2009.
(78) Note that for **XL** with APF-D, a small residual imaginary mode was present irrespective of the selected computational parameters.
(79) Hay, P. J.; Wadt, W. R. *J. Chem. Phys.* **1985**, *82*, 270.
(80) Hay, P. J.; Wadt, W. R. *J. Chem. Phys.* **1985**, *82*, 284.
(81) Tomasi, J.; Mennucci, B.; Cammi, R. *Chem. Rev.* **2005**, *105*, 2999−3094.
(82) Bylaska, E. J.; de Jong, W. A.; Govind, N.; Kowalski, K.; Straatsma, T. P.; Valiev, M.; van Dam, J. J.; Wang, D.; Apra, E.; Windus, T. L.; Hammond, J.; Autschbach, J.; Aquino, F.; Nichols, P.; Hirata, S.; Hackler, M. T.; Zhao, Y.; Fan, P.-D.; Harrison, R. J.;Dupuis, M.; Smith, D. M. A.; Glaesemann, K.; Nieplocha, J.; Tipparaju, V.; Krishnan, M.; Vazquez-Mayagoitia, A.; Jensen, L.; Swart, M.; Wu, Q.; Van Voorhis, T.; Auer, A. A.; Nooijen, M.; Crosby, L. D.; Brown, E.; Cisneros, G.; Fann, G. I.; Fruchtl, H.; Garza, J.; Hirao, K.; Kendall, R.; Nichols, J. A.; Tsemekhman, K.; Wolinski, K.; Anchell, J.; Bernholdt, D.; Borowski, P.; Clark, T.; Clerc, D.; Dachsel, H.; Deegan, M.; Dyall, K.; Elwood, D.; Glendening, E.; Gutowski, M.; Hess, A.; Jaffe, J.; Johnson, B.; Ju, J.; Kobayashi, R.; Kutteh, R.; Lin, Z.; Littlefield, R.; Long, X.; Meng, B.; Nakajima, T.; Niu, S.; Pollack, L.; Rosing, M.; Sandrone, G.; Stave, M.; Taylor, H.; Thomas, G.; van Lenthe, J.; Wong, A.; Zhang, Z. NWChem, A. *Computational Chemistry Package for Parallel Computers*, Version 6.1 (2012 developer's version). Pacific Northwest National Laboratory, Richland, WA,99352−0999, USA., 2012.
(83) Tamblyn, I.; Refaely-Abramson, S.; Neaton, J. B.; Kronik, L. *J. Phys. Chem. Lett.* **2014**, *5*, 2734−2741, DOI: 10.1021/jz5010939.
(84) Du, H.; Fuh, R. A.; Li, J.; Corkan, A.; Lindsey, J. S. *Photochem. Photobiol.* **1998**, *68*, 141−142; spectra available at http://omlc.ogi.edu/spectra/PhotochemCAD/ (last accessed: April 4, 2013) and at http://www.fluorophores.tugraz.at/ (last accessed: April 4, 2013).
(85) Magalhaes, J. L.; Pereira, R. V.; Triboni, E. R.; Berci Filho, P.; Gehlen, M. H.; Nart, F. C. *J. Photochem. Photobiol. A: Chem.* **2006**, *183*, 165−170.
(86) There was an error in the values reported for B3LYP in that original work; it has been corrected here.
(87) For fluorescence, Santoro and co-workers reported that the accuracy of the intensities in the stick spectrum to be more sensitive to the accuracy (ν^3 dependency) than their absorption counterpart,[25,27,28] which in turn could affect after convolution the positions of the bands.
(88) For the sake of clarity, we have used the same numbering as in previous works for the molecules belonging to this 0−0 benchmark set, but added the **00**- prefix to avoid confusion with the molecules used in the vibronic set. Note that many compounds are common to both sets.
(89) Wiggins, P.; Gareth Williams, J. A.; Tozer, D. J. *J. Chem. Phys.* **2009**, *131*, 091101.
(90) Plötner, J.; Tozer, D. J.; Dreuw, A. *J. Chem. Theory Comput.* **2010**, *6*, 2315−2324.
(91) Guido, C. A.; Mennucci, B.; Jacquemin, D.; Adamo, C. *Phys. Chem. Chem. Phys.* **2010**, *12*, 8016−8023.